Analytica Chimica Acta 1027 (2018) 101–108

Contents lists available at ScienceDirect

Analytica Chimica Acta

journal homepage: www.elsevier.com/locate/aca

Fluorescence-based immunosensor using three-dimensional CNT network structure for sensitive and reproducible detection of oral squamous cell carcinoma biomarker

Chung Kil Song [a, b], Eunkyul Oh [a], Min Sung Kang [a], Bum Seok Shin [a], Soo Young Han [a], Mingi Jung [a], Eui Seok Lee [c], Soo-Young Yoon [d], Myung Mo Sung [a], Wei Beng Ng [e], Nam-Joon Cho [e], Haiwon Lee [a, b, *]

[a] Department of Chemistry, Hanyang University, Seoul, 04763, South Korea
[b] Institute of Nano Science & Technology, Hanyang University, Seoul, 04763, South Korea
[c] Department of Oral and Maxillofacial Surgery, Korea University Guro Hospital, Seoul, 08308, South Korea
[d] Department of Laboratory Medicine, Korea University College of Medicine, Seoul, 08308, South Korea
[e] School of Materials Science and Engineering, Nanyang Technological University, 50 Nanyang Avenue, 639798, Singapore

HIGHLIGHTS

- Fluorescence-based immunoassay using 3DN-CNTs for OSCC biomarker detection.
- Detection sensitivity enhances due to high surface area and structural properties of 3DN-CNTs.
- Reproducible detection of biomarker results from uniform surface modification.

GRAPHICAL ABSTRACT

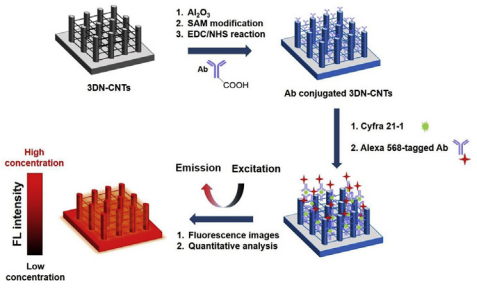

ARTICLE INFO

Article history:
Received 5 January 2018
Received in revised form
6 April 2018
Accepted 12 April 2018
Available online 18 April 2018

Keywords:
Cyfra 21-1
Fluorescence-based immunoassay
Oral squamous cell carcinoma
3DN-CNTs
Biosensor

ABSTRACT

A hierarchical three-dimensional network of carbon nanotubes on Si pillar substrate (3DN-CNTs) was developed for the accurate detection of oral squamous cell carcinoma (OSCC) in clinical saliva samples. The 3DN-CNTs were uniformly coated with a layer of aluminum oxides to enhance structural stability during biomarker detection. Cytokeratin-19 antigen (Cyfra 21-1) was utilized as a model biomarker of OSCC for fluorescence-based immunosensor using 3DN-CNTs (3DN-CNTs sensor). The 3DN-CNTs sensor enhances the sensitivity of Cyfra 21-1 detection by increasing the density of immobilized antibody through high surface area of 3DN-CNTs and enhancing the accessibility of biomolecules through the ordered pathway of hierarchical structure. The reliable detection limit for sensing of Cyfra 21-1 was estimated as in the level of 0.5 ng/mL and the quantitative estimation of Cyfra 21-1 was analyzed by 4-parameter logistic (4-PL) model for curve-fitting analysis. Clinical applicability of 3DN-CNTs sensor was evaluated through correlation with the commercially available electrochemiluminescence (ECL) detection system in the hospital. The assay results of the two systems for clinical saliva samples showed a good

* Corresponding author. Department of Chemistry, Hanyang University, 222 Wangsimni-ro, Seongdong-gu, Seoul, 04763, South Korea.
E-mail address: haiwon@hanyang.ac.kr (H. Lee).

https://doi.org/10.1016/j.aca.2018.04.025
0003-2670/

linear correlation. The 3DN-CNTs sensor offers great potential for accurate diagnosis of OSCC using Cyfra 21-1 biomarker in clinical fluids.

1. Introduction

Oral squamous cell carcinoma (OSCC) is the most common cancer of the oral cavity and the leading cause of death in the developing countries, and the mortality rate of OSCC patients has not significantly changed in the past 30 years [1–4]. The survival rate of the diseases is in the range of 80–90% at an early stage, whereas it is as low as only 15–50% at advanced stages [5]. Early detection of OSCC is a critical issue for the long-term survival of patients and successful treatment of cancer. Histopathological examination and biopsy have been used for a long time as a representative method of OSCC diagnosis. However, these processes are slow and time-consuming as well as critical diagnosis requires the professional interpretation by experienced pathologists if cellular or molecular changes were detected [4,6–8]. According to advances in molecular biology, clinical evaluation using cancer biomarker is considered to be useful for early diagnosis and prognostic monitoring with histopathological examination. Cancer biomarkers such as antigens, DNA, mRNA and enzymes are an important indicator for staging the pathological progression of the disease, and protein markers are most commonly used for cancer diagnosis [9,10]. The level of several biomarkers such as carcinoembyonic antigen, squamous cell carcinoma, immunosuppressive acidic protein and cytokeratin 19 fragment (Cyfra 21-1) in blood sample of OSCC patients led to sensitive and accurate diagnosis [11–13]. In recent decades, salivary analysis for OSCC diagnosis has become an alternative tool to the serum testing because saliva collection is simple, safe, painless, non-traumatic and can be taken repeatedly. Many research groups have been identified potential biomarkers in saliva of OSCC patients using the genomics or proteomics approach, and they have been applied for diagnosis and prognosis of OSCC [14–17].

Immunoassay-based methods have been widely used to determine the biomarkers in tumor tissues and body fluids such as blood, saliva and urine. Several types of immunoassay such as enzyme-linked immunosorbent assay (ELISA), fluorescence-based immunoassay, electrochemical sensor, chemiluminescence immunoassay, and multiplexed bead platforms have been explored for diagnostics of disease [18–22]. Although immunoassays can provide a simple, selective and cost-effective method for clinical diagnosis, they still have drawbacks such as long incubation time (hours-days), poor precision and limiting sensitivity which depends on the affinity of antibody-antigen. An analysis of the current state of the art reveals an unmet medical need in the management of oral carcinoma. Thus, novel strategies have been extensively worked out in the context of analytical platforms as well as diagnostic tools for rapid, sensitive and reproducible detection of biomarkers [23–26]. Nanomaterials, which have one spatial dimension less than 100 nm, have taken center stage as promising materials for catalyst, drug delivery, and sensing application in recent years due to their unique physical and chemical properties [27]. Recently, nanoscale systems such as nanostructured microfluidic array, three-dimensional carbon microarrays, zinc oxide nanowire arrays on hierarchical graphene, and silicon nanowires sensor arrays have been spotlighted as the noteworthy approaches for sensitive cancer diagnosis using high surface area, electrical and optical properties of nanomaterials [28–31]. Our group introduced a hierarchical three-dimensional network of carbon nanotubes on Si pillar substrate**s** (3DN-CNTs) for filtration in microfluidic systems [32,33]. The 3DN-CNTs provide not only high surface area but also easy functionalization to immobilize antibodies on the modified surfaces of CNTs based nanostructures.

In the present work, we offer a fluorescence-based immunosensor using 3DN-CNTs as a template (3DN-CNTs sensor) for the detection of Cyfra 21-1 which is one of representative OSCC biomarkers in saliva. The template was uniformly coated with Al_2O_3 to maintain the structural stability during solution drying process. The hydroxyl groups on an Al_2O_3-coated template was modified with an aminosilane reagent by self-assembled monolayer (SAM) formation for immobilization of biomolecules. The efficacy of 3DN-CNTs sensor was evaluated by the quantitative analysis of Cyfra 21-1 using a sandwich-type immunoassay method with a fluorescence-based corresponding antibody. In order to assess the feasibility of clinical diagnosis of OSCC, the Cyfra 21-1 concentration in clinical saliva samples measured by 3DN-CNTs sensor was compared with the results measured by electrochemiluminescence (ECL) assay.

2. Materials and methods

2.1. Materials

$Fe(NO_3)_3 \cdot 9H_2O$ and 3-(2-aminoethylamino)propyldimethoxymethylsilane (AEAPDMS) were purchased from Junsei (Tokyo, Japan). Mo solution (ICP/DCP standard solution) was purchased from Aldrich Chemicals (Milwaukee, WI, USA). Phosphate buffer saline (PBS), bovine serum albumin (BSA), *N*-(3-dimethylaminopropyl)-*N*′-ethylcarbodiimide hydrochloride (EDC), *N*-hydroxysuccinimide (NHS), 4-nitrobenzaldehyde and Tween 20 were purchased from Sigma Aldrich (St. Louis, MO, USA). Mouse monoclonal Cyfra 21-1 antibody (#10-2689, capture antibody; #10-2732, detection antibody; #61-1064, HRP-conjugated detection antibody) and partially purified Cyfra 21-1 protein (#30-AC69) were purchased from Fitzgerald Industries International (Action, MA, USA). Alexa Fluor 568 and tetramethylbenzidine (TMB) substrate solution were purchased from Thermo Scientific (Waltham, MA, USA). All other reagents were of analytical grade and used without further purification.

2.2. Fabrication of 3DN-CNTs

The fabrication of 3DN-CNTs was carried out as described in the previous reports [33,34]. The Si pillar-patterned substrate (diameter: 2 μm; height: 5 μm, and a gap of pillars: 1.5 μm) was used for fabricating 3DN-CNTs. 3DN-CNTs were synthesized by thermal chemical vapor deposition system using NH_3 gas for 10 min followed by C_2H_2 gas at 850 °C for 20 min. The deposition of Al_2O_3 onto 3DN-CNTs was conducted for 150 cycles by using atomic layer deposition (ALD, Cyclic 4000, Genitech). The morphology of 3DN-CNTs and Al_2O_3-coated 3DN-CNTs was examined by field-emission scanning electron microscope (FE-SEM, Hitachi S4800) operated at a beam energy of 15 kV. Raman spectra of 3DN-CNTs were detected by a Renishaw TM1000 Raman spectrometer (Renishaw, UK) using an Ar laser (laser excitation wavelength = 514.5 nm).

2.3. Amine functionalization of Al_2O_3-coated 3DN-CNTs

Al_2O_3-coated 3DN-CNTs were functionalized with amine groups by self-assembly process of AEAPDMS for antibody immobilization. Briefly, the Al_2O_3-coated 3DN-CNTs were exposed to ultraviolet (UV)-activated oxygen in a UV-ozone chamber (Jaesung Engineering, UVC-30, Korea) for 30 min to remove organic contaminants and generate hydroxyl groups on the surface of Al_2O_3. They were dipped into 1% AEAPDMS solution (in non-hydrous toluene) for 3 h under nitrogen atmosphere followed by washing with non-hydrous toluene and absolute ethanol thoroughly. In order to confirm the formation of monolayer on the surface of templates after SAM modification, Al_2O_3-coated 2D Si substrates were also modified with the same procedures described above. The surface morphology of Al_2O_3-coated 2D Si substrates after SAM modification was identified by atomic force microscope (AFM, Park Systems, XE-100, KR), and the thickness of self-assembled aminosilane layer was measured by ellipsometer (Rudolph Research, Ellipsometer Auto EL-III, NJ, USA) with a wavelength of 632.8 nm. The amino group after SAM modification initiated by the imine formation reaction between 4-nitrobenzaldehyde and amine group was validated using a UV/Vis/NIR spectrometer (PerkinElmer, LAMBDA™ 1050, CA, USA) as described in the previous report [35]. The number of amino groups was calculated through Beer-Lambert equation using individual absorbance of 4-nitrobenzaldehyde (at λ_{max} 267 nm) after hydrolysis of 4-nitrobenzaldehyde conjugated each 2D Si substrate and 3DN-CNTs.

2.4. Determination of pair antibodies against Cyfra 21-1

The binding assay was performed on BLItz system (ForteBio, Pall Life Sciences, NY, USA) in order to identify the binding selectivity of paired antibodies against Cyfra 21-1. Prior to binding measurements, Anti-mouse IgG Fc Capture (AMC) biosensor (Fortebio, USA) was equilibrated for 10 min in PBS. After an initial baseline for 30 s, capture antibody was loaded onto the AMC-coated sensor for 120 s. The biosensor was washed for 30 s by flowing through PBS and Cyfra 21-1 was then associated with for 120 s, followed by washing for another 30 s in PBS. The detection antibody was associated with for 120 s, followed by dissociation for 120 s in PBS. Pair antibodies were identified as suitable for assay development using a BLItz Pro software.

2.5. Quantification of Cyfra 21-1 with 3DN-CNTs sensor

Capture antibody was immobilized onto the amine-functionalized Al_2O_3-coated 3DN-CNTs by EDC-NHS crosslinking reaction. Each 5 μL of 1 mM EDC and 4 mM NHS was added into 990 μL PBS (pH 7.4) containing 10 μg capture antibody for pre-reaction at room temperature for 15 min. The amine-functionalized Al_2O_3-coated 3DN-CNTs were placed in a 96 well plate and incubated in the 100 μL of antibody solution at 25 °C for 3 h. After the reaction, the 3DN-CNTs were washed with 0.1% Tween 20 in PBS (T-PBS) thoroughly to remove any excess reagents and non-binding capture antibodies. Capture antibody-immobilized 3DN-CNTs were incubated at 100 μL of eleven different concentration of Cyfra 21-1 in the range from 0.1 to 10,000 ng/mL for 1 h, subsequently washed with T-PBS to remove unbound biomarkers. Next, each 3DN-CNTs was incubated in 100 μL of 10 μg/mL of Alexa 568-tagged detection antibody solution, which was prepared using Alexa Fluor® 568 antibody labeling kit, for 1 h and then non-binding antibodies were washed out. The fluorescence microscope images of 3DN-CNTs at different concentrations of Cyfra 21-1 were obtained using a BX51W1 upright fluorescence microscope (Olympus, Tokyo, JapanJP) with a 50 × objective lens at an exposure time of 500 ms. The fluorescence images were analyzed with ImageJ software (US National Institutes of Health). In order to compare the sensitivity of 3DN-CNTs, the sandwich ELISA was employed at the above-mentioned concentrations of Cyfra 21-1 according to the general procedure suggested for sandwich ELISA (Abcam, Cambridge, MA, USA).

2.6. Assays of clinical saliva samples

The Cyfra 21-1 in clinical saliva samples were analyzed to assess the diagnostic feasibility and capability of fluorescence-based 3DN-CNTs immunoassay method. The 11 saliva samples were collected from 4 healthy persons and 7 OSCC patients at the Department of Oral and Maxillofacial Surgery, Korea University Hospital. The clinical study was approved by the Institutional Review Board (IRB) at the hospital. Consent documents were also obtained from all patients included in this study.

The saliva samples were centrifuged at 12,000 g for 5 min, and the supernatants were passed through a 0.45 μm pore-sized syringe filter (Millipore, Bedford, MA, USA). The clear supernatants were aliquoted and frozen for storage at −80 °C until thawed for analysis. All experiments were performed within 2 weeks after sampling. The samples were thawed in room temperature until completely thawed. Non-diluted clinical samples were assayed using a commercially available ECL assay system (ARCHITECT, Abbott Laboratories, USA). The clinical samples were diluted two fold with PBS buffer for the assay of the 3DN-CNTs sensor and the results were compared with those determined by the ECL assay method.

2.7. Statistical analysis

All data expressed as means ± SD are representative of at least two different experiments. To estimate the possible systematic bias and analytical agreement between the fluorescence-based 3DN-CNTs sensor and ECL assay, Passing–Bablok regression analyses were performed on clinical data using the MedCalc program (Ostend, Belgium).

3. Results and discussion

3.1. Structural properties and stabilization of 3DN-CNTs

The hierarchical CNT networks on Si substrates prepared as a sensor template to increase the sensitivity of biomarker measurement. As shown in Fig. 1a, CNTs were synthesized on Si pillar-patterned substrates and interconnected in a hierarchical shape between adjacent pillars. The interconnected CNTs between pillars were observed in various shapes such as straight, arch and double y-junction between pillars and the mean diameter of single CNTs bundles connected between pillars was about 10–15 nm (Fig. S1c). The Raman spectra showed that the synthesized-CNTs were composed of single-walled carbon nanotubes (SWNTs) assembled in a bundled structure and the diameter of SWNTs was calculated to be about 0.9 nm as reported previously (Fig. 1c and d) [32,33].

The hierarchical morphology of CNTs between adjacent pillars was aggregated due to Van der Waals interaction and capillary force between adjacent CNTs during solution drying process [34]. Thin aluminum oxide layer was grown on the surface of 3DN-CNTs by atomic layer deposition (ALD) technique in order to achieve mechanical and structural stability of the hierarchical CNT networks. Fig. 1b showed the morphology of 3DN-CNTs after Al_2O_3 coating and the diameter of CNT bundle coated with Al_2O_3 was estimated to be 35 ± 5 nm (Fig. S1d). The hierarchical morphology of 3DN-CNTs was well maintained in aqueous solutions during the

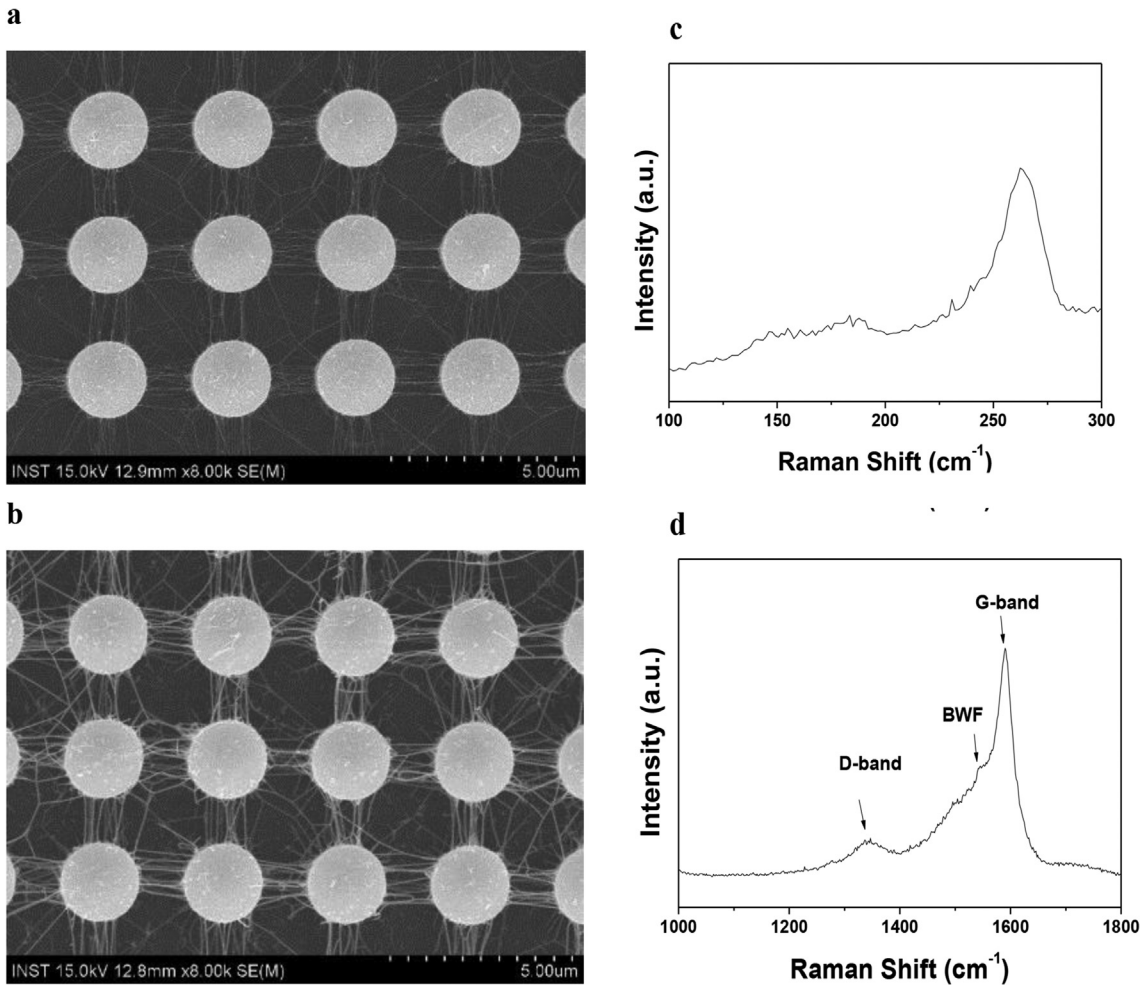

Fig. 1. The SEM images of (a) 3DN-CNTs and (b) 3DN-CNTs after ALD coating with Al_2O_3. (c) and (d) Raman spectra of 3DN-CNTs are an enlarged view of the RBM frequency range and the G/D frequency range, respectively. The wavelength of the excitation lasers is 514.5 nm.

surface modification, immobilization processes or biomarker assay after Al_2O_3 coating (Fig. S2). These results indicated that Al_2O_3-coated 3DN-CNTs can be utilized as a template for biomolecule recognition under solution phases.

3.2. Surface functionalized template for antibody immobilization

Reliable biosensor platforms require the reproducibility and stability of antibodies, the uniform density of antibodies on the attached surface, as well as the uniform structure of sensor templates. Organosilane self-assembled monolayer (SAM) is commonly used for surface modification of Si substrates. In this study, one of dialkoxysilane monomers (AEAPDMS) was chosen to generate monolayer formation and amine functionalization on the surface of templates for uniform immobilization of antibody on the Al_2O_3-coated 3DN-CNTs [35,36]. In order to get a preliminary clue for expounding the formation of monolayer on the 3DN-CNTs, the surface properties of Al_2O_3-coated 2D Si substrate after SAM modification were characterized by using ellipsometer and AFM. The measured thickness of aminosilane layer on a Si substrate after 3 h of SAM modification was 11 ± 1 Å which was close to the theoretical thickness of AEAPDMS monolayer. Fig. 2a and b showed 1.0 μm × 1.0 μm AFM images of Al_2O_3-coated 2D Si substrate and AEAPDMS modified Al_2O_3-coated 2D Si substrate after SAM modification, respectively. Non-contact mode AFM images did not show any aggregated multilayer formation after SAM modification. The RMS value of Al_2O_3-coated 2D Si substrate was 0.186 nm and it was similar to RMS values after SAM modification. The amine group on the surface after SAM was characterized by imine formation reaction between the amine group and 4-nitrobenzaldehyde. The absorbance values of 4-nitrobenzaldehyde at aminosilanized 2D Si substrate and 3DN-CNTs were converted into 0.89 and 2.40 of the amine groups in 100 $Å^2$, respectively. The absolute amine density of 3DN-CNTs after SAM modification was about 2.70 times higher than that of 2D Si substrate. On the basis of these results, the resultant layer on 3DN-CNTs after SAM modification was regarded as quasi-monolayer with successfully functionalized amine groups on the surface. The uniform modification of 3DN-CNTs can offer the reproducibility of antibody layer after immobilization of antibody.

3.3. The quantitative analysis of Cyfra 21-1 using 3DN-CNTs sensor

Scheme 1 illustrated the fluorescence-based immunoassay using 3DN-CNTs for the quantitative analysis of Cyfra 21-1. Paired antibodies against Cyfra 21-1 were selected by the binding assay using BLItz system which measures the shift in the interference pattern of the reflected light between the biomolecule-binding layer and an internal reference layer on a disposable fiber optic-based surface (Fig. 3). Various concentrations of Cyfra 21-1 in PBS solution were captured on the surface of 3DN-CNTs through

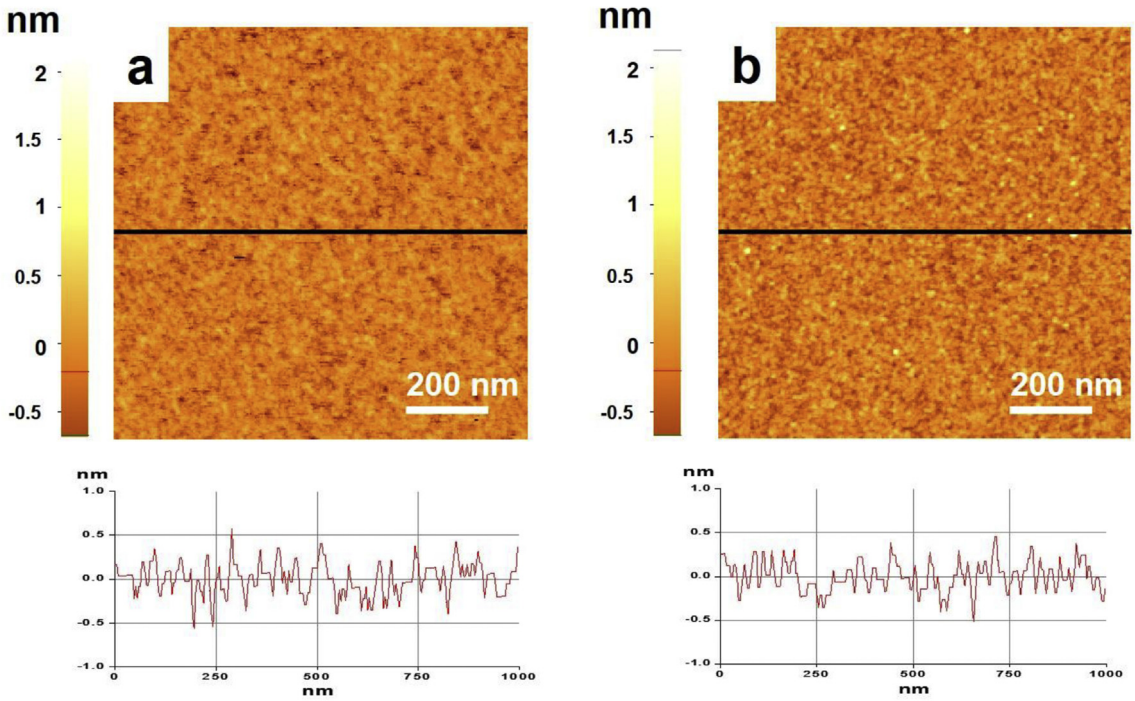

Fig. 2. Non-contact mode AFM images (top) and cross-sectional profiles (bottom) of (a) Al_2O_3-coated 2D Si substrate and (b) Al_2O_3-coated 2D Si substrate after SAM modification (3 h). The scan size is 1.0 μm × 1.0 μm. The RMS roughness is about 0.185 nm for (a) and (b).

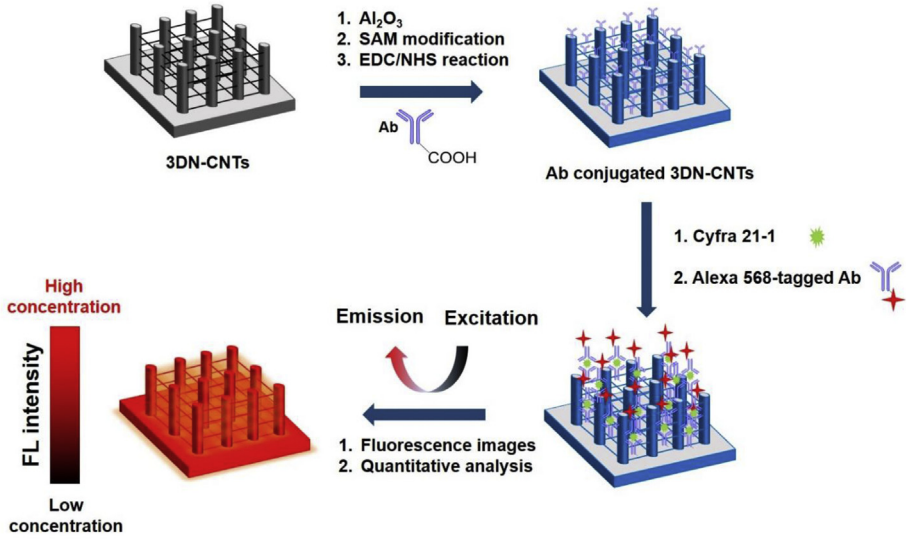

Scheme 1. Schematic illustration of the 3DN-CNTs sensor for Cyfra 21-1 detection.

antibody-antigen interaction, and Alexa-fluor 568-tagged antibodies were formed sandwich immunocomplexes. Fig. 4a showed that the fluorescence intensity was significantly enhanced with increasing concentrations of Cyfra 21-1 in the range from 1 to 1000 ng/mL. The fluorescence intensity values on each fluorescence image were converted into fluorescence enhancement ratio (F/F_0) and then plotted on a calibration curve with log scale of concentration (x-axis). As shown in Fig. 4b, the calibration curve is the sigmoidal in shape ranged from 0.1 to 10,000 ng/mL and the calibration curve was used for quantitative estimation of Cyfra 21-1 b y 4-parameter logistic (4-PL) model for curve-fitting analysis [37]. The adjusted R-squared of the experimental data according to 4-PL model is 0.993. The limit of detection (LOD) of Cyfra 21-1 measured by 3DN-CNTs sensor was found to be 0.5 ng/mL and it was

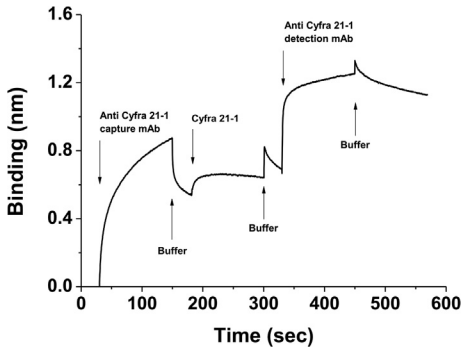

Fig. 3. Bio-layer interferometer binding analysis of pair antibodies against Cyfra 21-1.

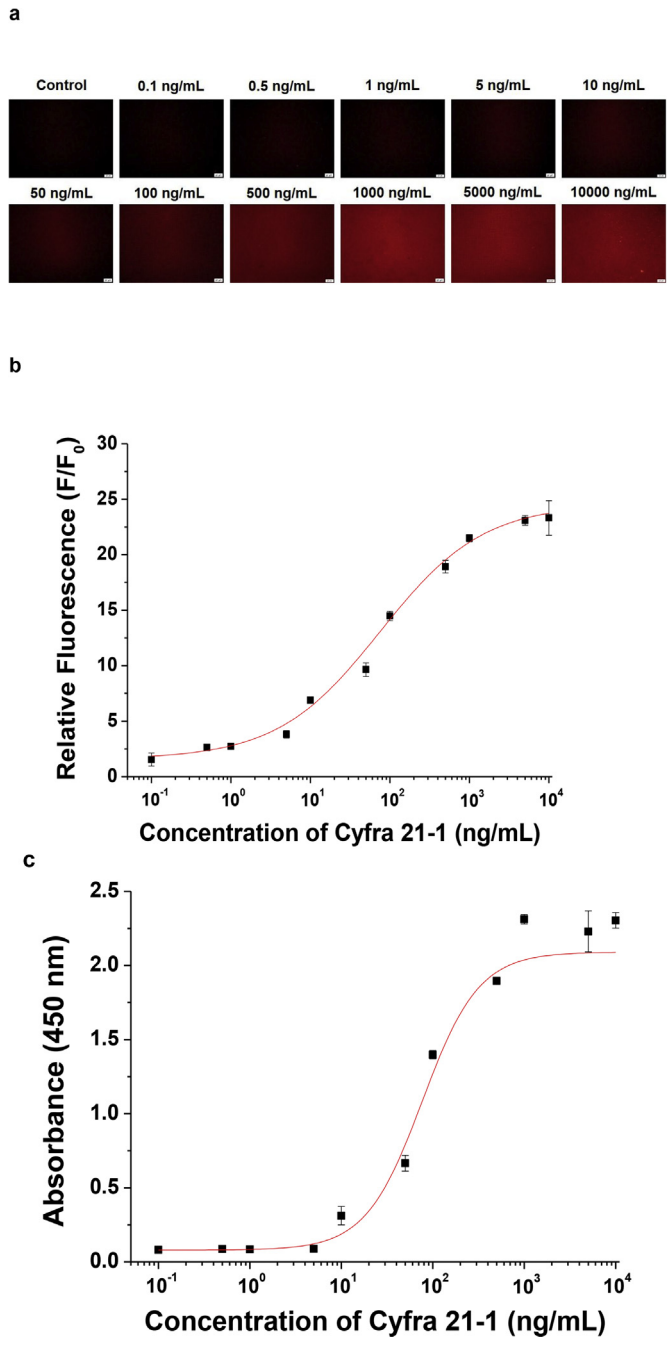

Fig. 4. Representative fluorescence images of (a) 3DN-CNTs sensor at different concentrations of Cyfra 21-1. (b) The calibration curve for Cyfra 21-1 on 3DN-CNTs sensor. (c) The standard calibration curve from a conventional sandwich ELISA.

determined by 3.3 times higher than the standard deviation of blank. The precision of the 3DN-CNTs sensor was evaluated by repeatedly assaying using coefficients of variation (CVs, n = 3). As shown in Table 1, the 3DN-CNTs sensor above LOD was shown to be with a CVs below 10%, and the CVs of 3DN-CNTs sensors at 1–1000 ng/mL of Cyfra 21-1 was 2.38–8.60%. The CVs results range from 1 to 1000 ng/mL were shown in reliable reproducibility for Cyfra 21-1 measured by 3DN-CNTs sensor. In addition, the sensitivity of 3DN-CNTs sensor was compared with a conventional ELISA method using same pair antibodies and antigen. The sensitivity of 3DN-CNTs sensor was approximately 20 times higher than that of the sandwich ELISA (Fig. 4c). The sensitivity enhancement of 3DN-CNTs sensor could be caused by increasing the maximum number of capture antibody on the surface because the total binding sites of 3DN-CNTs were estimated about three times higher than that of 2D Si substrate. In addition, the hierarchical structure of 3DN-CNTs increases the accessibility of biomolecules through the ordered pathways of 3DN-CNTs templates.

For clinical trials, the performance of 3DN-CNTs sensor in saliva samples (4 healthy persons and 7 OSCC patients) was compared with that of a commercially available ECL assay system. The ECL assay data of healthy persons (sample 1 to 4) were estimated at ranged from 2.6 to 4 ng/mL and those of OSCC patients (samples 5 to 11) were estimated at ranged from 4.2 to 62.5 ng/mL. The quantitative estimation of Cyfra 21-1 in saliva samples measured by 3DN-CNTs sensor was consistent with those of ECL assay within clinical range. Table 2 showed that the analytical precision of 3DN-CNTs sensors in clinical samples was evaluated by the CVs and the Mean CVs were estimated to be 11.92%. The similarity of two analytical methods was performed with Passing and Bablok regression analysis for 3DN-CNTs sensors *versus* ECL assay. The statistical procedure is a suitable non-parametric regression analysis and allows estimation of variation and systematic for comparative studies between two different analytical methods [38,39]. Fig. 5 showed no significant deviation from linearity (Cusum test for linearity; P = 0.77) and scatter point (black circle) and regression line (blue) of the results were included within 95% confidence intervals (CIs). These results indicated that two different analytical methods had good conformity and were valid for clinical saliva samples in the range from 1 to 62.5 ng/mL. As demonstrated herein, 3DN-CNTs biosensor could be proposed as a complementary sensor for the ECL assay with the limitation of quantitative analysis of some biological materials caused by a quenching effect.

4. Conclusions

In this study, sensitive and reproducible 3DN-CNTs sensor was developed for the detection of Cyfra 21-1 as OSCC biomarker. The surface of Al_2O_3-coated 3DN-CNTs was uniformly modified with amine groups for facilitating antibody immobilization. Potential application 3DN-CNTs as fluorescence-based immunosensor was investigated through quantitative analysis of Cyfra 21-1. The LOD of the 3DN-CNTs sensor was estimated to be 0.5 ng/mL and the calibration curve of Cyfra 21-1 was sigmoidal in shape ranged from 0.1 to 10,000 ng/mL with r square = 0.993. The sensitivity of 3DN-CNTs sensor was approximately 20 times higher than that of the conventional sandwich ELISA system. The 3DN-CNTs sensor improved the detection sensitivity of Cyfra 21-1 because of unique structural properties such as increase of total binding sites, hierarchical

Table 1
The mean value, SD, and CVs of fluorescence enhancement ratio (F/F_0) according to Cyfra 21-1 concentration measured by the 3DN-CNTs sensor.

Cyfra 21-1 (ng/mL)	Fluorescence enhancement ratio (F/F_0)		
	Mean value	Standard deviation	CVs, %
0.1	1.54	0.58	37.55
0.5	2.64	0.19	7.07
1	2.76	0.11	4.12
5	3.85	0.26	6.11
10	6.52	0.44	6.79
50	9.09	0.74	8.18
100	13.88	0.98	7.03
500	18.96	0.45	2.38
1000	23.28	2.00	8.60
5000	24.56	1.65	6.70
10,000	24.98	2.27	9.07

※ CVs: coefficient of variations.

Table 2
Comparison of Cyfra 21-1 concentration in 11 clinical saliva samples measured by ECL assay and 3DN-CNTs sensor.

Sample No.	ECL assay	3DN-CNTs sensor		
	Cyfra 21-1 (ng/mL)	Cyfra 21-1 (ng/mL)	Standard deviation	CVs, %
1	2.6	1.64	0.29	17.99
2	3.2	1.24	0.14	11.58
3	3.6	3.65	0.26	7.10
4	4	3.20	0.57	17.77
5	4.2	2.04	0.20	9.73
6	4.2	0.83	0.18	22.22
7	4.4	2.02	0.20	10.03
8	8.1	8.03	0.75	9.32
9	42.9	36.80	3.40	9.25
10	44.8	43.72	1.44	3.30
11	62.5	59.76	7.68	12.85

※ CVs: coefficient of variations.

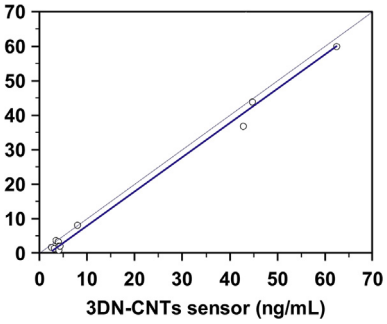

Fig. 5. Passing and Bablok regression analysis (a) between 3DN-CNTs sensor and ECL assay.

structures for the easy accessibility of biomolecules. The clinical feasibility of 3DN-CNTs sensors was assessed by comparing with commercial available ECL assay system in the hospital. The results of Cyfra 21-1 in saliva samples measured by 3DN-CNTs sensor showed a linear relationship and good conformity with those measured by ECL assay, and the mean CVs values of 3DN-CNTs sensors were less than 15% (CV cut-off value). The 3DN-CNTs sensor could be expected as a feasible biosensor for diagnosis of OSCC in clinical saliva samples. However, since the number of clinical samples analyzed by 3DN-CNTs biosensors is small and the commercially available ECL assay for OSCC diagnosis is not reliable enough to completely complement, further experiments will increase the reliability by using more patient samples in future study.

Acknowledgements

This work was supported by the National Research Foundation (NRF) grants funded by the Korean government (MSIP) (No. 2012M3A7B4035286). This work also supported by the MSIT (Ministry of Science and ICT), Korea, under the ITRC (Information Technology Research Center) support program (IITP-2017-1711055214) supervised by the IITP (Institute for Information & communications Technology Promotion). This work was also supported by Basic Science Research Program (No. 2012R1A6A1029029) through the NRF funded by the Ministry of Education. Funding was also provided by the grant (FA2386-15-1-4081) from the AFOSR/AOARD, USA.

Appendix A. Supplementary data

Supplementary data related to this article can be found at https://doi.org/10.1016/j.aca.2018.04.025.

References

[1] P.P. Dos Reis, R.R. Bharadwaj, J. Machado, C. MacMillan, M. Pintilie, M.A. Sukhai, B. Perez-Ordonez, P. Gullane, J. Irish, S. Kamel-Reid, Claudin 1 overexpression increases invasion and is associated with aggressive histological features in oral squamous cell carcinoma, Cancer 113 (2008) 3169–3180.
[2] D. Marsh, K. Suchak, K.A. Moutasim, S. Vallath, C. Hopper, W. Jerjes, T. Upile, N. Kalavrezos, S.M. Violette, P.H. Weinreb, Stromal features are predictive of disease mortality in oral cancer patients, J. Pathol. 223 (2011) 470–481.
[3] W.K. Mydlarz, P.T. Hennessey, J.A. Califano, Advances and perspectives in the molecular diagnosis of head and neck cancer, Expert Opin. Med. Diagn. 4 (2010) 53–65.
[4] B.T. Hill, L.A. Price, Lack of survival advantage in patients with advanced squamous cell carcinomas of the oral cavity receiving neoadjuvant chemotherapy prior to local therapy, despite achieving an initial high clinical complete remission rate, Am. J. Clin. Oncol. Cancer Clin. 17 (1994) 1–5.
[5] A.K. Markopoulos, E.Z. Michailidou, G. Tzimagiorgis, Salivary markers for oral cancer detection, Open Dent. J. 4 (2010) 172.
[6] O. Brinkmann, D.A. Kastratovic, M.V. Dimitrijevic, V.S. Konstantinovic, D.B. Jelovac, J. Antic, V.S. Nesic, S.Z. Markovic, Z.R. Martinovic, D. Akin, Oral squamous cell carcinoma detection by salivary biomarkers in a Serbian population, Oral Oncol. 47 (2011) 51–55.
[7] J.D. Holmes, E.J. Dierks, L.D. Homer, B.E. Potter, Is detection of oral and oropharyngeal squamous cancer by a dental health care provider associated with a lower stage at diagnosis? J. Oral Maxillofac. Surg. 61 (2003) 285–291.
[8] C. Scully, J.V. Bagan, C. Hopper, J.B. Epstein, Oral cancer: current and future diagnostic techniques, Am. J. Dent. 21 (2008) 199–209.
[9] S.M. Hanash, S.J. Pitteri, V.M. Faca, Mining the plasma proteome for cancer biomarkers, Nature 452 (2008) 571.
[10] A.M. Hawkridge, D.C. Muddiman, Mass spectrometry–based biomarker discovery: toward a global proteome index of individuality, Annu. Rev. Anal. Chem. 2 (2009) 265–277.
[11] H. Kurokawa, Y. Yamashita, S. Tokudome, M. Kajiyama, Combination assay for tumor markers in oral squamous cell carcinoma, J. Oral Maxillofac. Surg. 55 (1997) 964–966.
[12] L.P. Zhong, H.G. Zhu, C.P. Zhang, W.T. Chen, Z.Y. Zhang, Detection of serum Cyfra 21-1 in patients with primary oral squamous cell carcinoma, Int. J. Oral Maxillofac. Surg. 36 (2007) 230–234.
[13] G. Rosati, F. Riccardi, A. Tucci, Use of tumor markers in the management of head and neck cancer, Int. J. Biol. Markers 15 (1999) 179–183.
[14] R. Nagler, G. Bahar, T. Shpitzer, R. Feinmesser, Concomitant analysis of salivary tumor markers-a new diagnostic tool for oral cancer, Clin. Canc. Res. 12 (2006) 3979–3984.
[15] W.R. Kuo, K.W. Lee, K.Y. Ho, S.M. Tsai, F.Y. Chiang, K.H. Juan, Tissue polypeptide antigen, carcinoembryonic antigen, carbohydrate antigen, and CA125 levels as tumor markers in squamous cell carcinoma of the head and neck, Kaohsiung J. Med. Sci. 15 (1999) 152–158.
[16] M. Krimmel, J. Hoffmann, C. Krimmel, C.P. Cornelius, N. Schwenzer, Relevance of SCC-Ag, CEA, CA 19.9 and CA 125 for diagnosis and follow-up in oral cancer, J. Cranio-Maxillo-Fac. Surg. 26 (1998) 243–248.
[17] R.M. Nagler, Saliva as a tool for oral cancer diagnosis and prognosis, Oral Oncol. 45 (2009) 1006–1010.
[18] J.R. Lakowicz, Radiative decay engineering: biophysical and biomedical applications, Anal. Biochem. 298 (2001) 1–24.
[19] Y. Li, J. Sun, L. Wu, J. Ji, X. Sun, Y. Qian, Surface-enhanced fluorescence immunosensor using Au nano-crosses for the detection of microcystin-LR, Biosens. Bioelectron. 62 (2014) 255–260.
[20] J. Lin, H. Ju, Electrochemical and chemiluminescent immunosensors for tumor markers, Biosens. Bioelectron. 20 (2005) 1461–1470.
[21] X. Liu, Q. Dai, L. Austin, J. Coutts, G. Knowles, J. Zou, H. Chen, Q. Huo, A one-step homogeneous immunoassay for cancer biomarker detection using gold

nanoparticle probes coupled with dynamic light scattering, J. Am. Chem. Soc. 130 (2008) 2780–2782.
[22] J.C. Miller, H. Zhou, J. Kwekel, R. Cavallo, J. Burke, E.B. Butler, B.S. Teh, B.B. Haab, Antibody microarray profiling of human prostate cancer sera: antibody screening and identification of potential biomarkers, Proteomics 3 (2003) 56–63.
[23] H. Chon, S. Lee, S.W. Son, C.H. Oh, J. Choo, Highly sensitive immunoassay of lung cancer marker carcinoembryonic antigen using surface-enhanced Raman scattering of hollow gold nanospheres, Anal. Chem. 81 (2009) 3029–3034.
[24] S. Gibot, M.C. Béné, R. Noel, F. Massin, J. Guy, A. Cravoisy, D. Barraud, M. De Carvalho Bittencourt, J.P. Quenot, P.E. Bollaert, Combination biomarkers to diagnose sepsis in the critically ill patient, Am. J. Respir. Crit. Care Med. 186 (2012) 65–71.
[25] R. Fan, O. Vermesh, A. Srivastava, B.K. Yen, L. Qin, H. Ahmad, G.A. Kwong, C.C. Liu, J. Gould, L. Hood, Integrated barcode chips for rapid, multiplexed analysis of proteins in microliter quantities of blood, Nat. Biotechnol. 26 (2008) 1373–1378.
[26] T. Kaya, T. Kaneko, S. Kojima, Y. Nakamura, Y. Ide, K. Ishida, Y. Suda, K. Yamashita, High-sensitivity immunoassay with surface plasmon field-enhanced fluorescence spectroscopy using a plastic sensor chip: application to quantitative analysis of total prostate-specific antigen and GalNAcβ1–4GlcNAc-linked prostate-specific antigen for prostate cancer diagnosis, Anal. Chem. 87 (2015) 1797–1803.
[27] P. Pandey, M. Datta, B. Malhotra, Prospects of nanomaterials in biosensors, Anal. Lett. 41 (2008) 159–209.
[28] R. Malhotra, V. Patel, B.V. Chikkaveeraiah, B.S. Munge, S.C. Cheong, R.B. Zain, M.T. Abraham, D.K. Dey, J.S. Gutkind, J.F. Rusling, Ultrasensitive detection of cancer biomarkers in the clinic by use of a nanostructured microfluidic array, Anal. Chem. 84 (2012) 6249–6255.
[29] V. Penmatsa, A.R. Ruslinda, M. Beidaghi, H. Kawarada, C. Wang, Functionalized three-dimensional carbon microarrays for cancer biomarker detection, ECS Trans. 45 (2013) 7–14.
[30] H.Y. Yue, S. Huang, J. Chang, C. Heo, F. Yao, S. Adhikari, F. Gunes, L.C. Liu, T.H. Lee, E.S. Oh, ZnO nanowire arrays on 3D hierarchical graphene foam: biomarker detection of Parkinson's disease, ACS Nano 8 (2014) 1639–1646.
[31] G. Zheng, F. Patolsky, Y. Cui, W.U. Wang, C.M. Lieber, Multiplexed electrical detection of cancer markers with nanowire sensor arrays, Nat. Biotechnol. 23 (2005) 1294.
[32] T.J. Lee, J. Seo, H. Lee, J.W. Lee, W. Yi, Fabrication of single-walled carbon nanotube three-dimensional networks inside the pores of a porous silicon structure, Carbon 48 (2010) 1473–1479.
[33] J. Seo, T.J. Lee, S. Ko, H. Yeo, S. Kim, T. Noh, S. Song, M.M. Sung, H. Lee, Hierarchical and multifunctional three-dimensional Network of carbon nanotubes for microfluidic applications, Adv. Mater. 24 (2012) 1975–1979.
[34] K.G. Lee, S. Lee, S.J. Chang, B.G. Choi, J. Seo, A. Sangalang, D.H. Kim, T.J. Park, M.K. Lee, S.J. Lee, H. Lee, Bio-inspired hierarchical nanowebs for green catalysis, Small 11 (2015) 4292–4297.
[35] J.H. Moon, J.H. Kim, K.J. Kim, T.H. Kang, B. Kim, C.H. Kim, J.H. Hahn, J.W. Park, Absolute surface density of the amine group of the aminosilylated thin layers: ultraviolet– visible spectroscopy, second harmonic generation, and synchrotron-radiation photoelectron spectroscopy study, Langmuir 13 (1997) 4305–4310.
[36] J.H. Moon, J.W. Shin, S.Y. Kim, J.W. Park, Formation of uniform aminosilane thin layers: an imine formation to measure relative surface density of the amine group, Langmuir 12 (1996) 4621–4624.
[37] J.W. Findlay, R.F. Dillard, Appropriate calibration curve fitting in ligand binding assays, AAPS J. 9 (2007) E260–E267.
[38] H. Passing, W. Bablok, A new biometrical procedure for testing the equality of measurements from two different analytical methods. Application of linear regression procedures for method comparison studies in clinical chemistry, Part I, Clin. Chem. Lab. Med. 21 (1983) 709–720.
[39] L. Bilic-Zulle, Comparison of methods: passing and Bablok regression, Biochem. Med. 21 (2011) 49–52.